JOURNAL OF SOLID STATE CHEMISTRY **138,** 207–219 (1998)
ARTICLE NO. SC977601

Electronic Band Structure Calculations of the *M*N*X* (*M* = Zr, Ti; *X* = Cl, Br, I) System and Its Superconducting Member, Li-Doped β-ZrNCl

P. M. Woodward and T. Vogt

Physics Department, Brookhaven National Laboratory, Upton, New York 11973

Received May 29, 1997; in revised form August 12, 1997; accepted August 19, 1997

Electronic band structure calculations have been performed for β-ZrNCl, β-ZrNBr, α-ZrNBr, α-ZrNI, and α-TiN*X* (*X* = Cl, Br, I) using the extended Hückel method. These calculations reveal that *n*-doped β-ZrNCl has a single narrow band at the Fermi level which is stabilized by overlap of $4dz^2$ orbitals on zirconium with respect to the remainder of the conduction band states. This band shows only a small degree of dispersion and can essentially be described as a localized Zr–Zr bond when the carrier concentrations are low. The calculated band structure is consistent with the experimental observations of activated carrier transport, and an indirect optical band gap in β-ZrNCl and β-ZrNBr. A simple picture is presented which describes a mechanism for strong electron-phonon coupling in the β-ZrN*X* structure, suggesting that β-Li$_x$ZrNCl is a classical BCS superconductor. This localized $4dz^2$ band at the Fermi level is absent in the electronic band structures of α-ZrN*X* and α-TiN*X* compounds. The dispersion relations for these compounds show a direct optical band gap, as observed experimentally. The absence of significant metal–metal bonding in α-*M*N*X* compounds implies that *n*-doping will be more difficult to achieve in compounds adopting this structure. The relative stability of α- and β-polymorphs is also discussed.

Key Words: **extended Hückel calculations; electronic band structure; nitride halides; superconductivity.**

INTRODUCTION

Recently superconductivity was observed below 11.5 K in lithium intercalated β-ZrNCl (1). Superconductivity in intercalated materials is very attractive because the carrier concentration can be adjusted without introducing disorder-induced scattering. Such scattering, which arises when substitutional dopants are introduced onto electronically active sites in the crystal, often has a detrimental effect on the conduction properties. Another interesting feature is the structure of β-ZrNCl, which contains buckled ZrN layers that are somewhat similar to the CuO layers in the high T_c cuprate superconductors. However, zirconium is an early transition metal so that in contrast to the cuprates where the *d*-orbitals are nearly filled, here the *d*-orbitals are nearly empty.

β-ZrNCl and the isostructural compound β-ZrNBr (space group = $P\bar{3}$) were first synthesized and structurally characterized in the 1960's (2, 3). These compounds have two-dimensional structures with slabs containing the layer sequence *X*-Zr-N-N-Zr-*X*. These slabs are held together by halogen–halogen van der Waals interactions. Both compounds have structural polytypes, α-ZrNCl and α-ZrNBr (although α-ZrNCl is difficult to prepare and isolate as a pure phase and has not been well characterized), which adopt the FeOCl structure (space group = *Pmmn*) (2). This structure also contains slabs held together by halogen–halogen van der Waals forces, but the intralayer geometry and bonding in the α structure are distinctly different from the geometry and bonding in the β structure. Additionally, ZrNI and TiN*X* (*X* = Cl, Br, I) were also synthesized at the same time, but were found to exist only in the α-polymorph. The existence of these phases which are compositionally and structurally closely related to β-ZrNCl raises the possibility that several compounds in this family may display superconductivity. Furthermore, as with the cuprates, the superconducting properties, such as T_c, may be very dependent upon subtle variations in the composition, doping, and structure. In order to guide further synthetic efforts and better understand the nature of superconductivity in these compounds, we have examined their hand structures in detail.

CALCULATIONAL DETAILS

Band structure calculations were performed using the program CAESAR for Windows, developed by Jingqing Ren, Weigen Liang, and Myung-Hwan Whangbo. The calculations performed by CAESAR are based on the extended Hückel method (4–7). The atomic parameters used in the calculations are given in Table 1. All atomic parameters used were taken from the default values in CAESAR, with

0022-4596/98 $25.00

TABLE 1

Exponents ζ_j and Valence Shell Ionization Potentials H_{ii} of Slater-Type Orbitals c_i Used in the Extended Hückel Calculations

Atom	χ_i	H_{ii} (eV)	ζ_1	ζ_2	c_1	c_2
Zr	5s	− 8.00	1.817	—	1	0
Zr	5p	− 5.40	1.776	—	1	0
Zr	4d	− 10.20	3.835	1.505	0.62242	0.57822
Ti	4s	− 8.97	1.500	—	1	0
Ti	4p	− 5.44	1.500	—	1	0
Ti	3d	− 10.81	4.550	1.6	0.43908	0.73966
N	2s	− 26.0	1.950	—	1	0
N	2p	− 13.4	1.950	—	1	0
Cl	3s	− 26.3	2.183	—	1	0
Cl	3p	− 14.2	1.733	—	1	0
Br	4s	− 22.07	2.588	—	1	0
Br	4p	− 13.10	2.131	—	1	0
I	5s	− 18.00	2.679	—	1	0
I	5p	− 12.70	2.322	—	1	0

Note. The *d* orbitals are represented by a double-ζ expansion of the Slater wavefunction. For a description of the way in which these parameters are used see Albright, Burdett, and Whangbo (20). For the off-diagonal matrix elements $H^{\text{eff}} = \langle c_i|H^{\text{eff}}|C_I\rangle$ the weighted formula was used (21).

the exception of the titanium parameters, which were taken from the literature (8). Bond valence calculations were performed with the program Eutax (9).

STRUCTURAL DESCRIPTION

When viewed along the *c*-axis the layered structure of β-ZrNCl is apparent (Figure 1a). The zirconium, nitrogen, and chlorine ions are segregated into planes which contain only a single atomic species. The layer repeat sequence is Cl–Zr–N–N–Zr–Cl, and within this six layer slab covalent and ionic interactions are responsible for binding the atoms to each other. Chlorine–chlorine van der Waals interactions hold these six layer slabs together, to form an extended solid along the *c*-direction.[1] The Cl–Zr, Zr–N, N–N, and Cl–Cl interlayer distances are 1.71, 0.43, 1.85, and 3.10 Å respectively. Note that the short distance between the zirconium and nitrogen layers implies that these two layers are nearly coplanar. The long distance between the chlorine layers is a consequence of the weak binding interactions across the van der Waals gap. In β-ZrNBr the Br–Zr, Zr–N, N–N, and Br–Br interlayer distances become 1.89, 0.41, 1.85, and 3.30 Å, respectively. Interestingly, the Zr–N and N–N interlayer distances undergo almost no change upon substitution of the larger bromine for chlorine.

Alternatively, the β-ZrNCl structure may be described beginning from a hexagonal close packing of anions. For a hexagonal close packed array the layer stacking sequence is ABABAB… . This repeat stacking sequence is observed for the nitride and chloride layers. However, the compositional stacking sequence is N–N–Cl–Cl–N–N–Cl–Cl–… , which when combined with the positional stacking sequence gives the sequence A(N)–B(N)–A(Cl)–B(Cl)–… . The structure is completed by placing zirconium in the octahedral holes which lie between the nitride and chloride layers, while the octahedral holes that lie between either two nitride or two chloride layers remain empty. Viewed from a traditional cation polyhedron model this gives layers of ZrN_3Cl_3 octahedra in which each octahedron shares six edges, all within the layer, to form edge sharing chains running along the **a**, **b**, and **a** + **b** directions (the local bonding geometry in β-ZrNCl is shown in Fig. 1b). This layered edge sharing octahedral network is analogous to the structures observed for the layered transition-metal dichalcogenides, 1T–MX_2 (M = Ti, Zr, V, Nb, Ta; X = S, Se, Te) (10). The structure of β-ZrNCl is distorted from this ideal picture, however, by the zirconium ions shifting out of the center of the octahedron toward the nitride face of the octahedron. The magnitude of this shift is 0.64 Å in β-ZrNCl and 0.74 Å in β-ZrNBr. This distortion is at least partially driven by the size difference between the nitrogen and halide ions. However, the short Zr–Zr distances, across the nitride faces of the octahedra, of 2.71 Å and 2.67 Å in β-ZrNCl and β-ZrNBr respectively,[2] imply a metal–metal bonding interaction between zirconium layers. This point will be discussed in more detail later.

The α-MNX (M = Ti, Zr; X = Cl, Br, I) structure is shown in Fig. 1c and 1d. Both β-MNX and α-MNX structures contain six layers of atoms in the sequence X–Zr–N–N–Zr–X which are held together by covalent and ionic bonding. Furthermore, these structural building blocks are held together in both polytypes by halogen–halogen van der Waals interactions. Both structures feature a distorted octahedral coordination about zirconium, and inspection of the α-ZrNBr and β-ZrNBr structures shows that the Zr–N and Zr–Br distances are very similar in the two polytypes. Comparing the two structures in greater detail however, reveals important differences. In the α-form zirconium is coordinated by four nitrogens and two halogens, rather than three neighbors of each type as found in the β-form. Additionally, the short metal–metal distance, characteristic of the β-polytype, is not present in the α-polytype. The effects of these changes in the nearest neighbor and next nearest neighbor coordination environments are reflected in the bond valences given in Table 2.

[1] Juza and Friedrichsen observed a high concentration of stacking faults in the stacking of chloride layers across the van der Waals gap (3).

[2] By comparison, the Zr–Zr distances in α-Zr are 3.18 Å and 3.23 Å, and 3.09–3.13 Å in the zirconium monohalides ZrCl and ZrBr, which show strong metal–metal bonding (22).

TABLE 2
The Bond Valences for *M*N*X* Compounds as Calculated Using the Program Eutax (9)

Compound	Metal	Nitrogen	Halogen	Total *M*–*M*
β-ZrNCl	4.22	3.09	1.13	1.48
β-ZrNBr	3.77	2.99	0.79	1.66
α-ZrNBr	4.11	3.45	0.65	1.24
α-ZrNl	4.51	3.53	0.98	1.31
α-TiNCl	4.32	3.25	1.06	1.11
α-TiNBr	4.20	3.43	0.77	1.41
α-TiNl	4.32	3.16	1.16	1.08

Note. The metal–metal bond valences given in the last column are the sum of a single *M*–*M* bond for the β-*M*N*X* compounds and four *M*–*M* bonds for the α-*M*N*X* compounds, and are not included in the bond valence values given for the metal in column 2.

The change in zirconium (titanium) coordination environment also has an effect on the halogen packing. The anion sublattice in α-ZrN*X* can no longer be described as having a close packed stacking sequence. Figure 2 illustrates the differences in the halogen layer packing in the α- and β-modifications. This change in packing causes an expansion in the *xy* plane and a contraction in the *z* direction in α-ZrN*X*. This can be quantified by calculating the density of atoms in each layer, and the distance between layers. Such calculations are summarized in Table 3 for *M*N*X* (*M* = Zr, Ti; *X* = Cl, Br, I). From this table one can clearly see the expansion in the layers of the α phases, which in turn allows the van der Waals gap to decrease significantly. The larger interlayer distances observed in β-ZrNCl and β-ZrNBr may facilitate intercalation.

RESULTS

The calculated electronic density of states (DOS) near the Fermi level is shown for β-ZrNCl in Fig. 3a. The results show a filled valence band and an empty conduction band, as expected based on the formal oxidation states of the constituent ions (Zr^{4+}, N^{3-}, Cl^{-}). The band gap is calculated to be 1.93 eV. Figures 3b–3d show the partial density of states (PDOS) contributions from zirconium, nitrogen, and chlorine. The PDOS curves reveal that the valence band contains roughly equal contributions from nitrogen 2*p* and chlorine 3*p* orbitals, and a smaller but significant contribution from zirconium. The presence of occupied zirconium levels can be attributed to covalency in the Zr–N and Zr–Cl interactions. The conduction band consists of electronic states originating on zirconium (primarily 4*d* orbitals).

Figure 4 shows the calculated DOS curves of β-ZrNCl, β-ZrNBr, α-ZrNCl, TiNCl, TiNBr, and ZrN for comparison. Table 4 gives the positions of the band edges and band gaps for *M*N*X* compounds. Among the *M*N*X* compounds the general features of the DOS curves are all quite similar. Changes in the band positions can mostly be attributed to changes in the electronegativity of the constituent ions. As the halogen ion becomes more electropositive, from Cl to Br to I, the top of the valence band steadily shifts to higher energy. In a similar fashion, substituting titanium for zirconium causes the bottom of the conduction band to shift to lower energy by approximately 1 eV. Both effects cause a decrease in the band gap, consistent with the observed changes in the colors of these compounds. Although qualitative agreement exist between the observed and calculated values, when compared with the experimentally determined band gap values, the calculated band gap energies are too small. This is not unexpected, as the extended Hückel method does not typically give accurate estimates of the band gap.[3]

Most of the changes in the DOS curves in Fig. 4 can be attributed to shifts in the band edges with changing composition. However, there is a clear difference between the DOS curves of compounds which adopt the β-ZrN*X* structure, and those which adopt the α-structure. In both β-ZrNCl and β-ZrNBr there is a narrow band present just below the main conduction band. This feature is not present in the DOS curves associated with any of the α-*M*N*X* compounds. The PDOS curves shown in Fig. 3, clearly show that this band has a significant contribution from the Zr 4*d* orbitals. The fact that this band is found at a lower energy than all of the other Zr 4*d* based bands in Fig. 4, is due to the stabilization energy which accompanies the bonding overlap of Zr 4*d* orbitals. Even stronger evidence for the enhanced metal–metal bonding overlap in the β-ZrN*X* structure is given in the crystal orbital overlap populations (COOP) plotted in Fig. 5 (11, 12). They show a strongly bonding Zr–Zr overlap in β-ZrNBr, which is populated upon *n*-doping. Furthermore, because the Zr–Zr bonding COOP is much larger than either the Zr–N or Zr–*X* antibonding COOP's, this suggests that *n*-doping will results in a net increase in the bonding overlap, and

[3]The underestimation of the band gaps in ZrN*X* compounds is somewhat surprising, considering that the EHTB technique normally overestimates the band gap values in oxides.

FIG. 1. The structures of β-ZrNBr and α-ZrNBr. (a) An extended view of β-ZrNBr along the *c*-axis; (b) the local bonding geometry in β-ZrNBr; (c) an extended view of α-ZrNBr along the *c*-axis; (d) the local bonding geometry in α-ZrNBr. The yellow spheres represent zirconium, the red spheres nitrogen, and the blue spheres bromine.

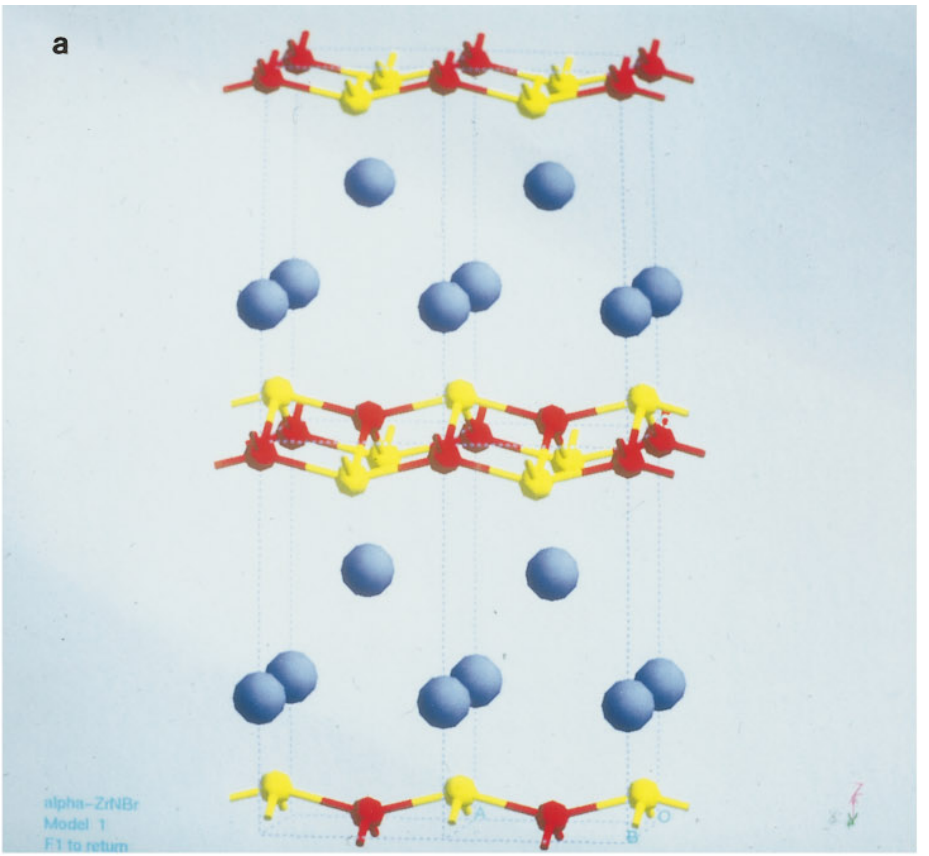
a
alpha–ZrNBr
Model 1
F1 to return
A
B
C

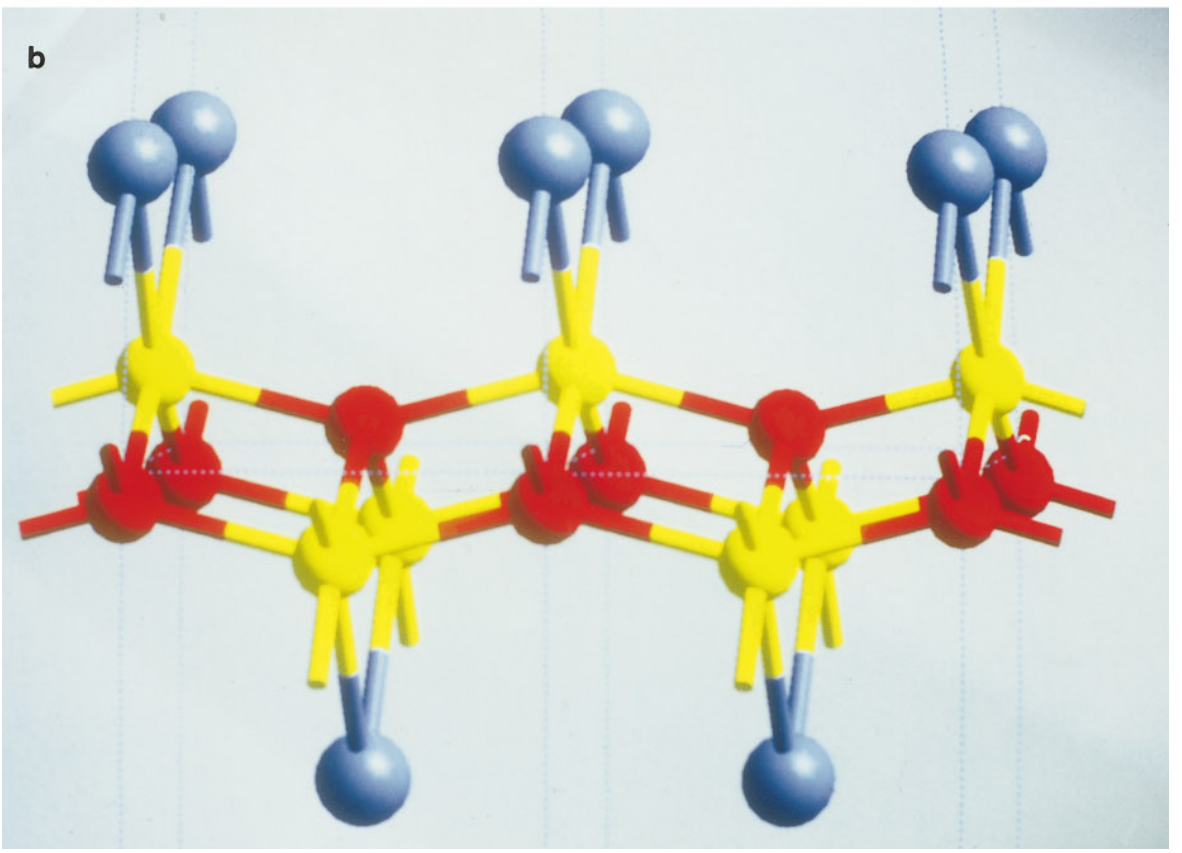
b

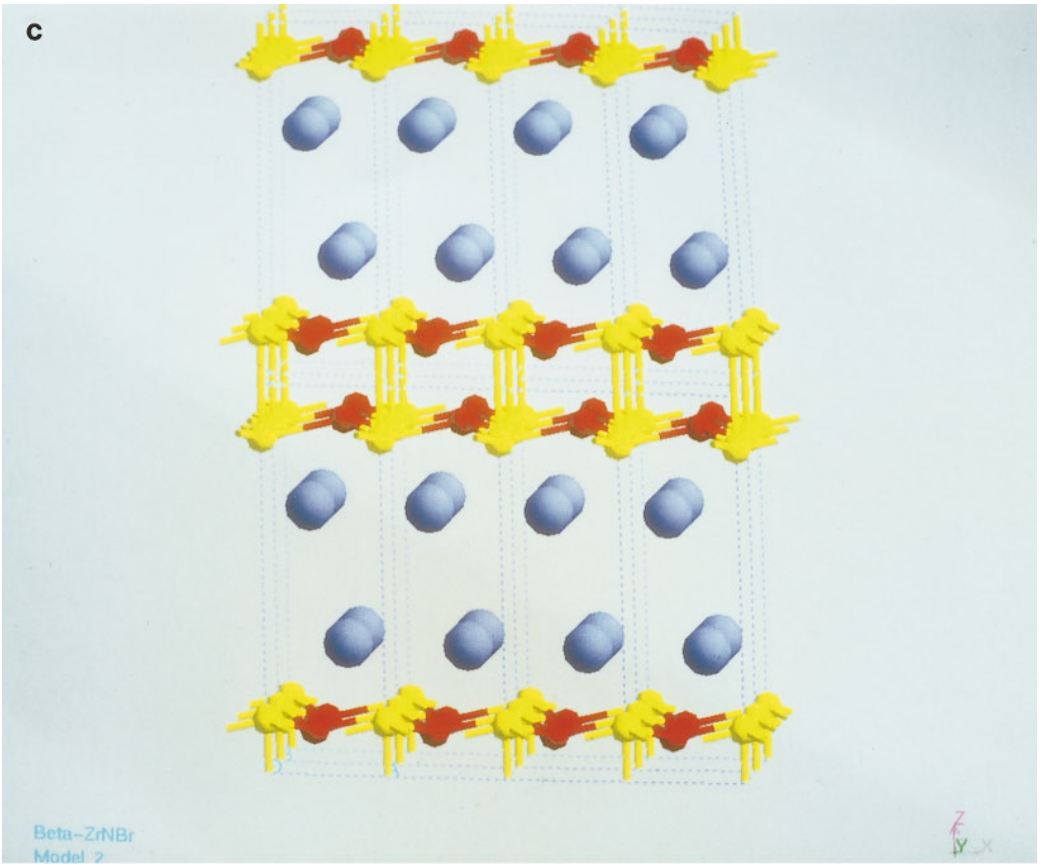
c
Beta-ZrNBr
Model 2

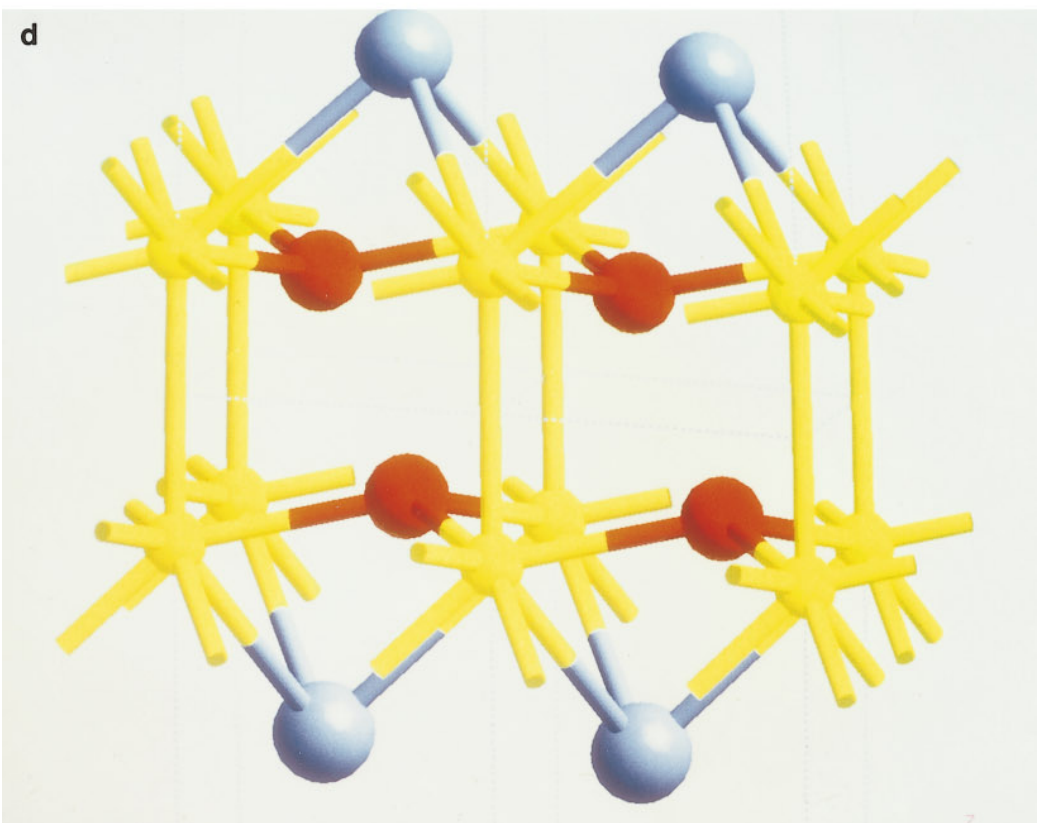
d

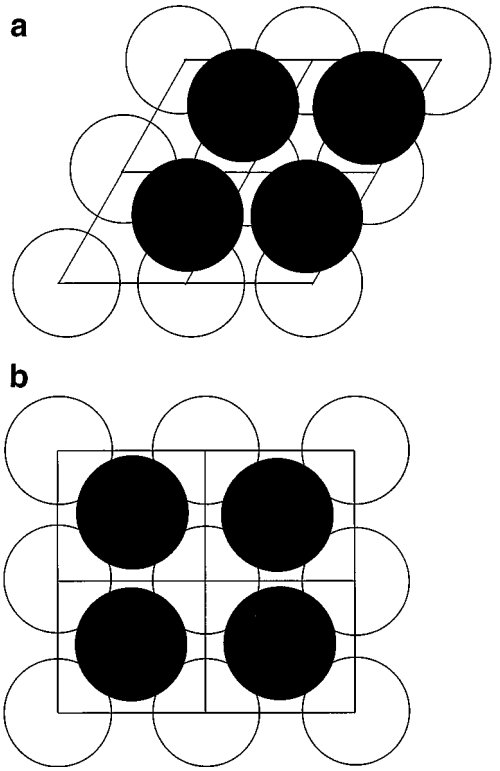

FIG. 2. A schematic representation of the halogen layer packing across the van der Waals gap in (a) the β-MNX structure and (b) the α-ZrNBr structure. The open circles represent the halogen ions in the lower and the filled circles the ions in the upper layer.

a subsequent stabilization of the total energy.[4] Figure 5 shows that *n*-doping in the α-polytype will also lead to population of metal–metal bonding orbitals. However, the bonding overlap is much smaller in the α-structure and is offset by the destabilizing influence of populating the *M*–N and *M*–*X* antibonding orbitals. Thus unlike β-Zr*NX* compounds, α-*MNX* compounds do not appear to be stabilized by *n*-doping.

The optical absorption spectra of Zr*NX* compounds show a sharp absorption edge for α-ZrNBr and α-ZrNI, whereas β-ZrNCl and β-ZrNBr show a more gradual increase in the optical absorption with decreasing wavelength (13). This behavior implies a direct band gap for the α-Zr*NX* structure and an indirect gap for the β-Zr*NX* structure. In order to compare these experimental observations with the calculated band structure, dispersion curves for *MNX* compounds were calculated and are shown for α-ZrNBr and β-ZrNCl in Fig. 6. Consistent with the optical measurements, these calculations show α-ZrNBr to be a direct gap semiconductor with the lowest energy transition occurring at the gamma point. β-ZrNCl also has a maximum valence band energy at the gamma point, but one of the two conduction band levels that are degenerate at the gamma point has an energy along the *X* to *M* direction, of approximately 0.5 eV below its energy at the gamma point.[5] Thus the EHTB calculations predict an indirect gap for β-ZrNCl consistent with the optical absorption spectra of this compound. In interpreting their optical spectra Ohashi, Yamanaka, and Hattori speculated that the moderate absorption from 475 to 370 nm (2.6–3.4 eV) may be caused by either an indirect transition or impurity levels. However, the EHTB calculations given here clearly indicate that this absorption is due to an intrinsic indirect transition. One additional feature evident in Fig. 6 is the lack of dispersion in the *Z*-direction, which indicates that the electronic band structure of these materials, like the crystal structure, is strongly two dimensional.

DISCUSSION

The most striking feature of these calculations is the observation of a narrow Zr–Zr bonding band below the main conduction band in β-ZrNCl and β-ZrNBr. The short distance between zirconium atoms at $0, 0, z$ and $0, 0, -z$ suggests significant overlap of the $4dz^2$ orbitals of neighboring atoms. In pure β-Zr*NX* these orbitals are unoccupied, and therefore no metal–metal bonding occurs. However, if electrons are introduced through *n*-doping, they would be expected to populate the Zr $4dz^2$ orbitals and form a Zr–Zr bond. One can quantitatively test this hypothesis using Mulliken population analysis to monitor changes in the populations of the various atomic orbitals as electrons are added to the unit cell. Performing this calculation for both β-ZrNCl and β-ZrNBr reveals that 91% of the added electron density resides on zirconium orbitals and 60% of the added electron density resides on Zr $4dz^2$ orbitals if the electron population is increased by one electron per zirconium ion.

If the Zr-based band in β-ZrNCl and β-ZrNBr was formed purely from overlap of $4dz^2$ orbitals to give a two center $2e^-$ bond, it should not show any dispersion. However, Fig. 6 reveals that the energy decreases by 0.5 eV upon moving from the Γ to the *X* point. Because the Zr–Zr distance within a plane is quite large ($\sim$3.6 Å), the spatial overlap of zirconium-based atomic

[4]The narrow Zr $4dz^2$ bond disappears in EHTB calculations carried out on a hypothetical two dimensional compound with only a single ZrNCl layer (no interlayer Zr–Zr bonding). The same calculations also show that for a doping level $0.5e^-$ per formula unit, the average energy of the conduction band electrons (doped carriers) is lower for the double layer β-ZrNCl structure. This result supports the conclusion that the Zr–Zr bonding stabilization outweighs the Zr–N and Zr–*X* antibonding interactions.

[5]The *X* point refers to the boundary of the Brillouin zone along [100], and the *M* point refers to the zone boundary along [110].

TABLE 3
Bond Distances (in Angstroms) and Interlayer Spacing in *MNX* Compounds

Compound	*M–M* distance	*M*–N distance	*M–X* distance	Intralayer *X–X* distance	Interlayer *X–X* distance	Atomic layer density (atoms/Å^2)	Van der Waals gap distance
β-ZrNCl	1×2.71	3×2.12	3×2.68	6×3.60	3×3.74	0.089	3.10
β-ZrNBr	1×2.67	3×2.12	3×2.82	6×3.64	3×3.91	0.087	3.30
α-ZrNBr	4×3.19	4×2.12	2×2.85	2×3.58 2×4.12	4×3.77	0.068	2.61
α-ZrNl	4×3.27	4×2.16	2×2.95	2×3.72 2×4.11	4×4.17	0.065	3.11
α-TiNCl	4×3.00	4×2.01	2×2.42	2×3.26 2×3.94	4×3.69	0.078	2.65
α-TiNBr	4×2.91	4×2.00	2×2.67	2×3.35 2×3.93	4×3.83	0.076	2.83
α-TiNI	4×3.01	4×2.02	2×2.74	2×3.52 2×3.94	4×4.23	0.078	3.31

Note. The atomic layer density is calculated for a single halogen layer in the crystal.

orbitals is too small to explain this dispersion. This implies that a small degree of mixing with the nitrogen and/or the halogen orbitals is responsible for the dispersion of this band.

How can the band structure calculations be reconciled with the structure and properties observed for both Li-doped β-ZrNCl and so-called "undoped" β-ZrN*X* samples. The bond distances and valences given in Tables 2 and 3

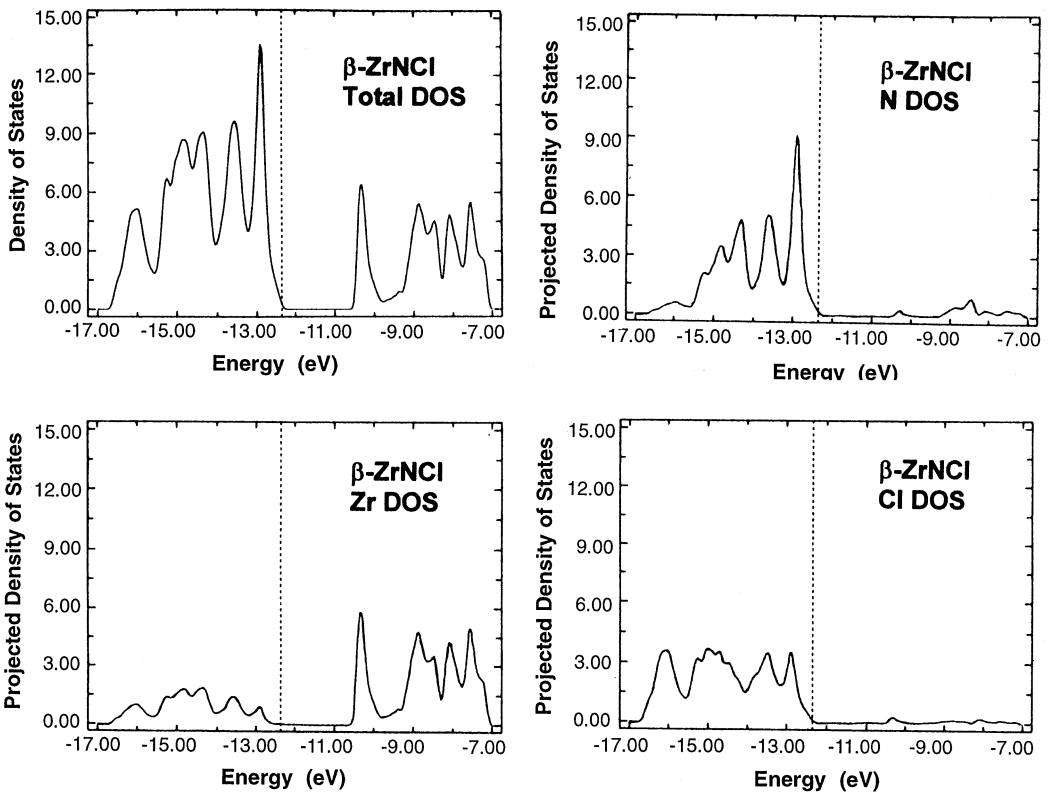

FIG. 3. The electronic density of states (DOS) for β-ZrNCl near the Fermi level. The remaining figures show the partial density of states (PDOS) curves for zirconium, nitrogen, and chlorine. The dotted line indicates the position of the Fermi level for a compound with no doping ($Z = 2$, $32e^-$ per unit cell).

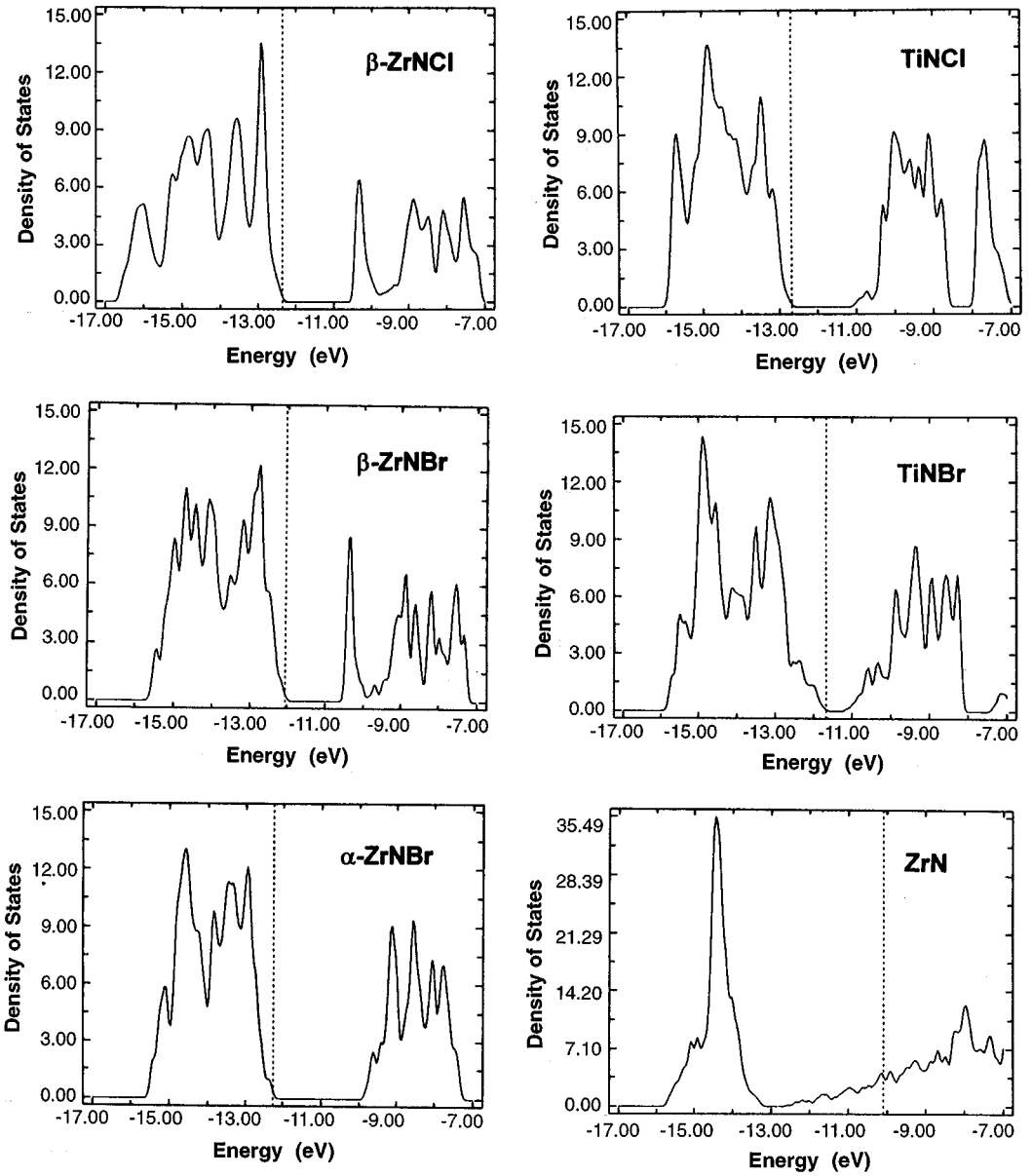

FIG. 4. The electronic density of states (DOS) curves near the Fermi level for severl MNX compounds and ZrN. The dotted line indicates the position of the Fermi level for a compound with no doping ($Z = 2, 32e^-$ per unit cell).

strongly suggest the presence of a Zr–Zr bond, despite the fact that the structures were determined on as-prepared, "undoped" samples, where the band structure calculations show that the $4dz^2$ orbitals should be empty. The optical properties observed for "undoped" β-ZrNCl and β-ZrNBr, are consistent with a transition from a filled valence band to an empty conduction band. However, transport measurements on the same samples show an activated transport of carriers with activation energies (0.10 eV for β-ZrNBr and 0.06 eV for β-ZrNCl) (13) much lower than expected from the optical band gaps. Furthermore, it has been noted that vapor transport synthesis of β-ZrNBr actually produces samples with compositions H_xZrNBr $(0.1 < x < 0.3)$ (13, 14). Both transport properties and bond distances are indicative of at least partial n-doping from intercalated protons, but the color is not black as seen when β-ZrNCl is doped with similar concentrations of lithium. This behavior is similar to the properties observed in ZnO samples doped with donor impurities in concentrations of less than one atomic percent (15). Zinc oxide when prepared in this way acts as a "transparent conductor," that is, a material which possesses high electrical conductivity while maintaining

TABLE 4
Calculated Band Edge Positions and Experimentally Determined Band Gaps (13) and Colors (2, 13) for *M*N*X* Compounds

Compound	Valence band maximum (eV)	Conduction band minimum (eV)	Calculated band gap (eV)	Band Gap at the Γ point (eV)	Observed band gap (eV)	Color
β-ZrNCl	−12.35	−10.42	1.93	2.58	2.6 (3.4)	Yellow-green
β-ZrNBr	−12.05	−10.43	1.62	2.21	3.2 (2.3)	Light yellow
α-ZrNBr	−12.25	− 9.82	2.43	2.43	2.9	Yellow
α-ZrNl	−11.93	− 9.90	2.03	2.03	2.4	Orange
α-TiNCl	−12.70	−11.00	1.70	1.70	—	Black
α-TiNBr	−11.67	−11.22	0.45	0.45	—	Black
α-TiNl	−11.50	−11.14	0.36	0.36	—	Black

a band gap in the visible or ultraviolet region of the spectrum. Such behavior in β-ZrNCl and β-ZrNBr samples prepared from vapor transport could be observed if a fraction of the intercalated hydrogen disassociated, donating its electrons to the Zr $4dz^2$ orbitals. The activated transport implies that the electrons are localized and move through the crystal via a hopping mechanism. Interpreting this behavior in light of the calculated band structure suggests a mechanism where the electrons are localized in Zr–Zr bonds and hop from filled Zr–Zr $4dz^2$ bonds to empty bonds via the nitrogen p_z orbitals.

When β-ZrNCl is doped with lithium to give β-Li$_x$ZrNCl ($x \sim 0.16$) it becomes black, shows metallic conductivity, and becomes superconducting below 11.5 K (1, 16). The changes in optical and transport properties with respect to β-H$_x$ZrNCl suggest much higher doping concentrations in the lithium doped samples. The crossover from activated to metallic conduction as the carrier concentration increases is not expected from the one-electron-band structure calculations presented here. Apparently when the concentration of occupied Zr–Zr bonds reaches a critical value the electrons in these bonds, and the local lattice distortions that accompany them, begin to interact. Above this critical concentration the electrons which were localized in Zr–Zr bonds at low concentrations become itinerant and display collective, metallic transport properties. Further studies of the structure and transport properties of *n*-doped β-ZrN*X* samples prepared as a function of doping concentration are necessary to better understand this behavior.

The presence of a Zr–Zr bond formed primarily form d_{z^2} orbitals was not anticipated in the crude band structure models previously proposed for these compounds, which suggested that the conduction band originated from the Zrt_{2g} orbitals (1, 13). However, the presence of this band explains many of the differences observed in the physical properties of α-*M*N*X* and β-*M*N*X* compounds. It explains the ease with which β-ZrN*X* compounds can be *n*-doped by intercalating lithium, and the presence of hydrogen interstitials in samples prepared from gas transport. The partial occupation of this band is also presumably responsible for the fact that β-*M*N*X* compounds are stable toward oxidation in air, whereas α-*M*N*X* compounds are relatively unstable in air. Furthermore, the fact that β-ZrN*X* compounds have much higher conductivities and lower activation energies than expected from their band gaps can be explained by a partially occupied Zr $4dz^2$ band. Finally, as already pointed out the indirect band gap observed for β-ZrNCl and β-ZrNBr corresponds to transitions from the valence band to this band.

This study also raises several interesting questions with regard to the structural stability of *M*N*X* compounds. There is obviously a competition between the α- and β-polytypes, and an examination of the factors stabilizing each structure is useful, particularly as a guide for future synthetic work on these compounds. Both polymorphs have similar *M*–N distances, but the α-polymorph has four *M*–N bonds to three for the β-polymorph. Since the *M*–N bonding is stronger than the *M*–*X* bonding (see the COOP curves in Fig. 5), the α-polymorph would on this basis be expected to be the lowest energy structure. Based on the increased number of short Zr^{4+}–N^{3-} interactions in the α-polymorph, ionic interactions should also favor the α-polymorph over the β-polymorph. This assumption is supported by Madelung energy calculations, performed with the program, Eutax (9), which give energies of −133.7 and −129.7 eV per formula unit for α-ZrNBr and β-ZrNBr, respectively. Yet β-ZrNBr is formed when α-ZrNBr, synthesized at 550–650°C, is heated to 850°C. This would seem to indicate that β-ZrNBr is the thermodynamically stable phase at high temperatures. How then can we understand this apparent stabilization of the β-polymorph with respect to the α-polymorph? In addition to the cation–anion bonding and the ionic interactions, there are two additional factors which must be taken into account: the degree of

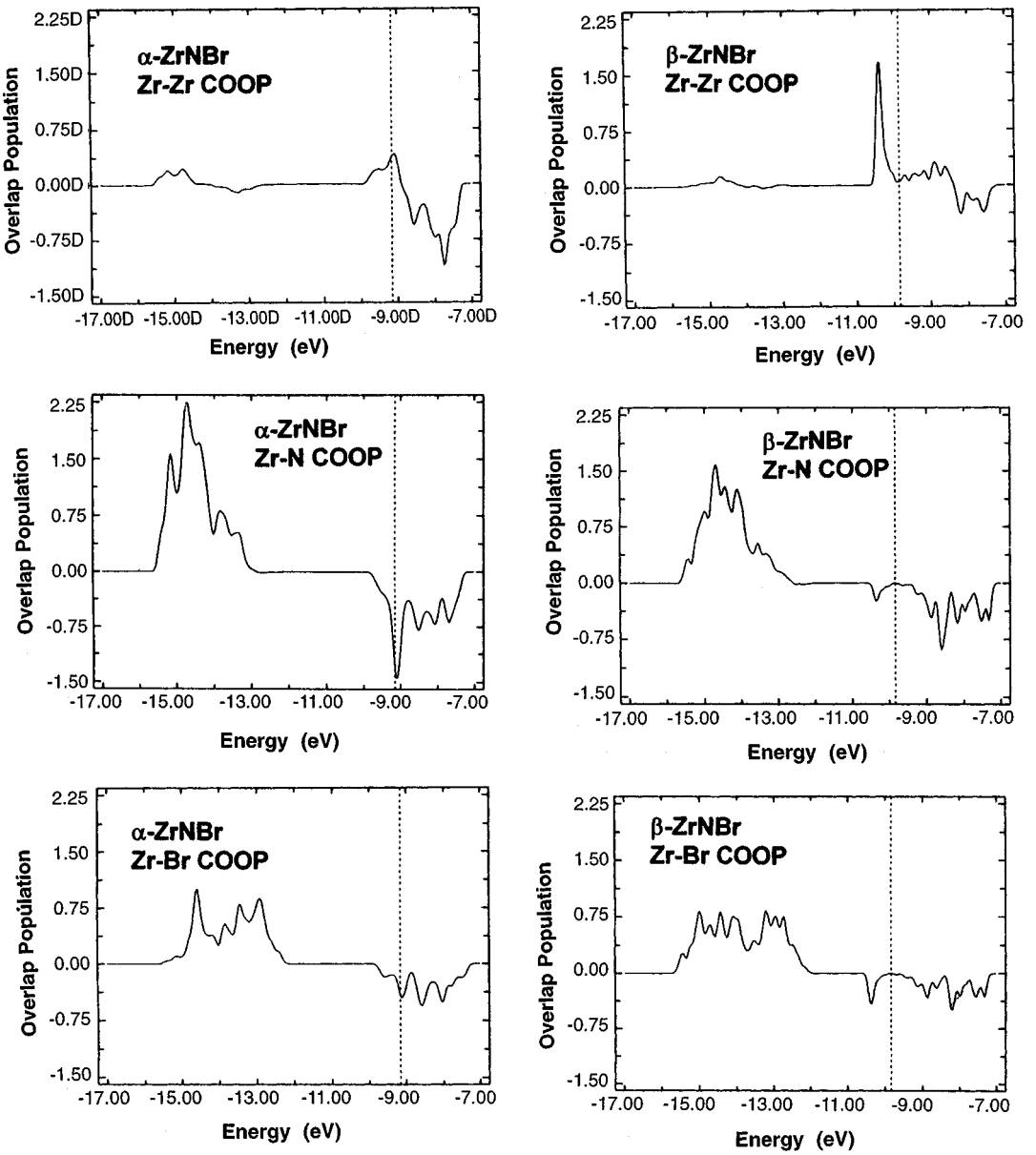

FIG. 5. The crystal orbital overlap population (COOP) curves for α-ZrNBr and β-ZrNBr. Positive values of overlap population indicate bonding interactions, negative values indicate antibonding interactions. The Fermi level for these figures corresponds an n-doping of one electron per zirconium ion ($Z = 2, 34e^-$ per unit cell).

metal–metal bonding and the size of the halogen ion. It is clear from the above discussion and the COOP curves shown in Fig. 5 that metal–metal bonding stabilizes the β-polytype. For tetravalent cations this stabilization will increase as the n-doping increases. Neglecting ionic interactions and considering only the energy of the valence electrons, as calculated by the extended Hückel method, Fig. 7 shows that at a doping level of 0.8 e^-/Zr β-ZrNBr becomes more stable than α-ZrNBr. The fact that the β-polytype is generally observed at much lower doping levels illustrates that this calculation is not to be taken quantitatively. Nonetheless, Fig. 7 does qualitatively illustrate the close competition between the two structures and the way in which n-doping stabilizes the β-polymorph.

The effect of halogen size is not as apparent, but was alluded to earlier. The metal nitrogen layers are fairly rigid and will only tolerate a small expansion in the M–N bond distance. Evidence for this exists not only in the nearly constant Zr–N and Ti–N bond distances across the entire series of compounds, but also in the very small expansions

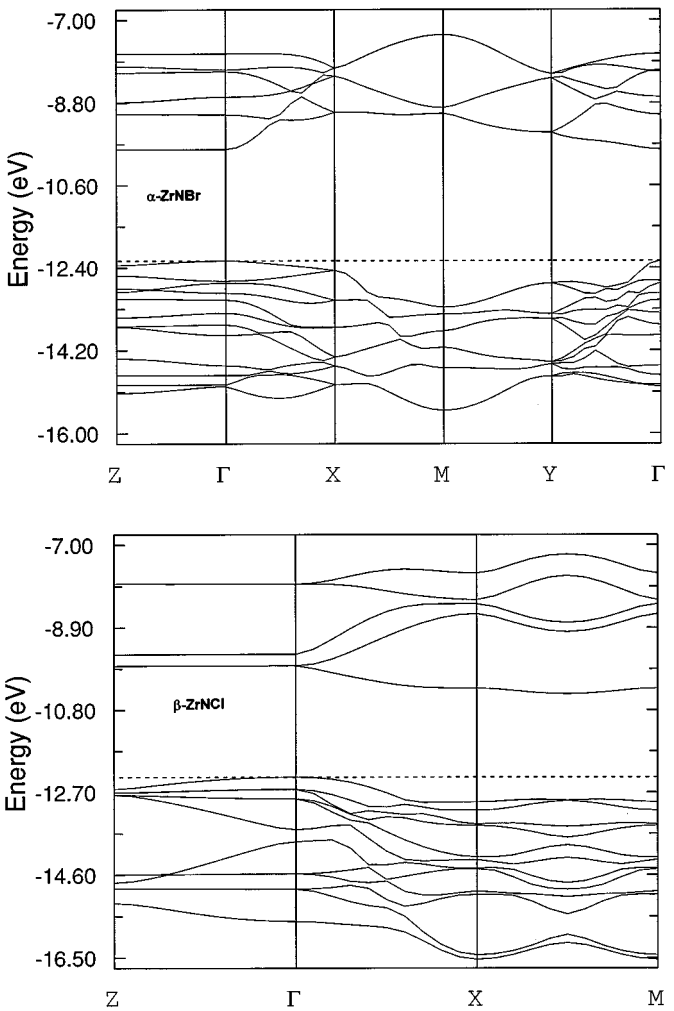

FIG. 6. Dispersion relations for α-ZrNBr and β-ZrNCl in an energy window near the Fermi level. The valence bands are primarily nitrogen $2p$ and halogen $3p$ ($4p$) in character, while the conduction bands are predominantly zirconium $4d$ in character. The dotted line indicates the position of the Fermi level for a compound with no doping ($Z = 2$, $32e^-$ per unit cell).

seen in the xy plane when the size of the halogen ion is changed. Therefore, the halogens must fit within the framework defined by the metal/nitrogen network. Table 3 shows that within a layer the atoms are more closely packed in the β-polytype. This is favorable for the smaller chlorine ions, but becomes increasingly restrictive as the size of the halogen increases. Thus we see that ZrNBr can readily be obtained in either polymorph, whereas ZrNI only exists in the α-polytype. The small size of titanium and the reduced spatial extent of its d orbitals both favor the α-polytype. This is consistent with the observation that no TiNX compound with the β-ZrNX structure is known.

How can the band structure calculations presented here be used to evaluate prospects for superconductivity in other MNX systems? First of all, based on its similarity to both the crystal and electronic band structure of β-ZrNCl, β-ZrNBr would be expected to display similar properties, including superconductivity. Preparation of superconducting n-doped β-ZrNBr would be very enlightening because the mass of the halogen ion would be significantly altered, while the Zr–N network and the electronic band structure near the Fermi level would be relatively unperturbed. This could provide insight into the role, if any, that the halogen ions play in these materials. It would be interesting to prepare β-NbNCl or β-TaNCl, which would have a filled dz^2 band just below the Fermi level, and then attempt to p-dope these compounds. The stabilization of the metal–metal bond would be fully realized in these d^1 systems, and therefore it is not unreasonable to expect that they should be stable compounds. Finally, although it is not clear from these calculations whether n-doped α-MNX compounds will show superconductivity, it is clear that n-doping will be much more difficult to achieve in the α-polymorph.

What do the band structure calculations reveal about the mechanism of superconductivity in β-ZrNCl? The σ overlap of Zr $4dz^2$ orbitals results in the formation of a localized chemical bond which shows little dispersion. For the doping levels observed in these compounds only some of the Zr–Zr bonding levels are occupied. The activated transport observed for lightly doped β-ZrNCl and β-ZrNBr is consistent with a picture of electrons hopping from occupied Zr–Zr bonding orbitals to empty Zr–Zr bonding orbitals. The weak dispersion that is observed for this band in the xy plane arises from mixing with N p_z orbitals and suggests that hopping occurs through Zr–N antibonding levels. Furthermore, when an electron hops from one site to another a change in the local geometry, in particular the Zr–Zr distance, is expected. This will produce a local lattice distortion, or polaron, which will move through the lattice with

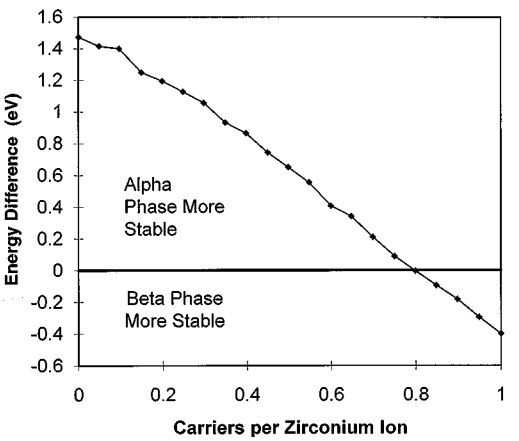

FIG. 7. The energy difference $E(\beta$-ZrNBr$)$–$E(\alpha$-ZrNBr$)$ in eV as a function of n-doping carrier concentration. The energies used represent the total energy of the valence electrons calculated by the extended Hückel method.

the electron. When the carrier concentration is increased in β-Li_xZrNCl the size of the polarons may be such that they overlap, leading to delocalization of electrons and metallic conductivity. This movement of Zr–Zr pairs toward each other when an electron hops into the Zr $4dz^2$ orbitals to form a bond, and away from each other when it leaves, corresponds to the stretching vibration of a Zr–Zr bond. Coupling of this lattice vibration with the electronic transport could easily be the strong electron–phonon coupling mechanism characteristic of a classical BCS superconductor. Variable temperature vibrational spectroscopy studies of these compounds would be highly desirable to better understand the relationship between lattice vibrations and transport properties in these materials.

It is also interesting to compare the band structure of β-ZrNCl with that of other superconducting materials such as ZrN, the high T_c cuprate superconductors, and the quaternary family of $Ln Ni_2B_2C$ (Ln = rare earth) superconductors. β-ZrNCl and ZrN have quite different electronic band structures, physical properties, and bonding interactions. ZrN is metallic and cubic in the normal state. Each zirconium ion is isotropically coordinated by 6 nitrogen neighbors and 12 next nearest zirconium neighbors at distances of 2.31 Å and 3.26 Å, respectively (17). Conversely, β-ZrNCl is semiconducting (at least from 300 to 150 K) and possesses a highly anisotropic two-dimensional structure. Each zirconium ion in β-ZrNCl is coordinated by three nitrogen, one zirconium, and three chlorine neighbors at distances of 2.12, 2.71, and 2.68 Å. Thus both the anisotropy and the covalency of Zr–N and Zr–Zr interactions are enhanced in β-ZrNCl. These differences in bonding are directly reflected in the electronic band structure. In ZrN the Fermi level is found in the middle of a broad π^* band, primarily of Zr t_{2g} character, whereas in n-doped β-ZrNCl the Fermi level is located in a narrow band formed primarily from a σ overlap of Zr $4dz^2$ orbitals.

Comparing the band structure of β-ZrNCl with the high T_c cuprate superconductors one finds that both materials are two-dimensional, show considerable cation–anion covalency, have contributions from a relatively small number of bands at the Fermi level, and can be doped with little perturbation of the electronic states near the Fermi level. However, in the cuprates, unlike β-ZrNCl, the partially filled band at the Fermi level is a σ^* band which originates from strong covalent interactions between neighboring cations and anions. It has been proposed that this is a key feature present in the electronic band structures of high T_c materials (18).

The quaternary $Ln Ni_2B_2C$ family of superconductors and β-ZrNCl share several common features. Structurally both can be described as layered structures with separated stacked anion layers. They have similar T_c's and in both families the density of states near the Fermi level has a large metal d-component, Zr 4d and Ni 3d respectively. As Mattheiss points out, the Ni–Ni bond length in $LuNi_2B_2C$ ($T_c \sim 17$ K) is smaller than observed in fcc nickel, indicating the presence of strong metal–metal bonding (18). The presence of metal–metal bonding interactions at the Fermi level in $LuNi_2B_2C$ and β-ZrNCl, rather than metal–anion σ-bonding interactions as in the cuprates, suggests that the mechanism of superconductivity in these materials is different from that in high T_c cuprate materials. Matthiess *et al.* have shown that in the $Ln Ni_2B_2C$ family of materials the electronic states near the Fermi level are sensitive to a high-frequency optical mode which dynamically modulates the NiB_4 tetrahedral bond angles. They propose that the superconducting properties of these materials are highly dependent upon this electron–phonon coupling, which indicates conventional superconducting behavior (19). From this comparison with $Ln Ni_2B_2C$ it would appear that β-ZrNCl is also a conventional superconductor. However, there are several differences between $Ln Ni_2B_2C$ compounds and β-ZrNCl which should be noted. In $LuNi_2B_2C$, rather than a single d orbital dominating the density of states near the Fermi level, all five Ni 3d orbitals contribute in roughly equal proportions. This results in a more three-dimensional band structure in $LuNi_2B_2C$. Also, the coexistence of superconductivity and long-range magnetic ordering separates this family from β-ZrNCl and the layered cuprates.

In conclusion, the electronic band structure results presented in this paper both answer interesting questions regarding the physical properties, particularly the electronic transport properties, of β-ZrNX compounds, and some more questions. Future work in the MNX family should provide interesting insights into the appearance of superconductivity in layered inorganic solids.

ACKNOWLEDGMENTS

We graciously acknowledge Jingqing Ren, Weigen Liang, and Myung-Hwan Whangbo for making possible the use of CAESAR, without which this work would not have been possible. We are also indebted to Dong-Kyun Seo for valuable discussions and a critical reading of this manuscript. This work was supported by the Division of Materials Sciences, U.S. Department of Energy, under Contract DE-AC02-76CH00016.

REFERENCES

1. S. Yamanaka, H. Kawaji, K. Hotehama, and M. Ohashi, *Adv. Mater.* **8,** 771 (1996).
2. V. R. Juza and J. Heners, *Z. Anorg. Allg. Chem.* **332,** 159–172 (1964).
3. V. R. Juza and H. Friedrichsen, *Z. Anorg. Allg. Chem.* **332,** 173–178 (1964).
4. R. Hoffmann, *J. Chem. Phys.* **39,** 1397 (1963).
5. R. Hoffmann and W. N. Lipscomb, *J. Chem. Phys.* **36,** 2179 (1962).
6. R. Hoffmann and W. N. Lipscomb, *J. Chem. Phys.* **37,** 2872 (1962).
7. M.-H. Whangbo and R. Hoffmann, *J. Am. Chem. Soc.* **100,** 6093 (1978).
8. J. K. Burdett and T. Hughbanks, *J. Am. Chem. Soc.* **106,** 3101–3113 (1984).

9. M. O'Keeffe, "Eutax. Program for Calculating Bond Valences." EMLab Software, Phoenix.
10. M.-H. Whangbo, D.-K. Seo, and E. Canadell, "Physics and Chemistry of Low-Dimensional Inorganic Conductors." C. Schlenker, J. Dumas, M. Greenblatt, and S. van Smaalen (Eds.), p. 285. Plenum, New York, 1996.
11. R. Hoffmann, "Solids and Surfaces: A Chemist's View of Bonding in Extended Structures." VCH, New York, 1988.
12. T. Hughbanks and R. Hoffmann, *J. Am. Chem. Soc.* **105,** 3528 (1983).
13. M. Ohashi, S. Yamanaka, and M. Hattori, *J. Ceram. Sco. Jpn. Int. Ed.* **97,** 1175 (1989).
14. M. Ohashi, H. Nakano, S. Yamanaka, and M. Hattori, *Solid State Ionics* **32/33,** 97 (1989).
15. R. Wang, A. W. Sleight, R. Platzer, and J. A. Gardner, *J. Solid State Chem.* **122,** 166 (1996).
16. M. Ohashi, S. Yamanaka, M. Sumihara, and M. Hattori, *J. Inclusion Phenom.* **2,** 289 (1984).
17. T. W. Baker, *Acta. Crystollogr.* **11,** 300 (1958).
18. L. F. Mattheiss, *Phys. Rev. B* **47,** 8224 (1993).
19. L. F. Mattheiss, T. Siegrist, and R. J. Cava, *Solid State Commun.* **91,** 587 (1994).
20. T. A. Albright, J. K. Burdett, and M.-H. Whangbo, "Orbital Interactions in Chemistry," Chap. 1. Wiley, New York, 1985.
21. J. Ammeter, H.-B. Bürgi, J. Thibeault, and R. Hoffmann, *J. Am. Chem. Soc.* **100,** 3686 (1978).
22. R. L. Daake and J. D. Corbett, *Inorg. Chem.* **16,** 2029 (1977).